RSC Advances

ROYAL SOCIETY OF CHEMISTRY

www.rsc.org/advances

Influence of the HDPE Molecular Weight and Content on the Morphology and Properties of the Impact Polypropylene Copolymer /HDPE Blends

Xuanbo Liu*, Xiaopei Miao, Meifang Guo, Wenbo Song and Jingbo Shao

Research Institute of Material Science, Beijing Research Institute of Chemical Industry, Beijing, 100013, People's Republic of China. E-mail: xuanboliu@hotmail.com; Tel: +86 10 59202920

Abstract

Two HDPE resins with different molecular weight were blended with one impact polypropylene copolymer with varied weight contents. The influence of molecular weight and content of PE on the morphology and properties of the blends were studied. It is found that by changing the molecular weight and weight content of PE, the morphology of the blends shows great difference. Spherical particles with different detail structures and obvious orientation structure were found. The properties such as impact strength and elongation at break depend not only the composition but also on the morphology. This study may shed light on the structure-property relationship study in the polyolefin impact blends.

Introduction

Polypropylene (PP) is widely-used in a variety of areas, known as a thermoplastic with excellent cost-to-performance ratio.[1] But the brittleness at low temperature or high deformation speed of the homo PP limits its application. The impact modifiers such as ethylene-propylene rubbers (EPRs), ethylene-propylene-diene copolymer (EPDM) and the other olefin copolymers are utilized to improve the toughness by compounding or in-reactor polymerization technology. The heterophasic materials of this kind are often called impact polypropylene copolymers (IPCs), which are extensively used in many areas such as automotive, housewares etc.

HDPE resins are often introduced in IPCs to purposely improve the properties by compounding with IPCs directly or multi-reactor polymerization process.[2-10] Correspondingly, the relationship between the structure and properties of this kind of multiphase materials has been intensively studied. The addition of HDPE was reported to influence the impact strength [2, 3, 6, 7, 9, 11, 12], minimize the magnitude of the modulus decrease[2, 3], suppress the stress-whitening[5, 7].

Mirabella studied the IPC/HDPE blends with HDPE weight percent 0~40%.[11] A monotonic decrease in flexural modulus was observed. The notched Izod impact strength (NIS) showed a maximum at HDPE content of 10 wt% and then the NIS decreased slightly with increasing HDPE content up to 40 wt%. The morphology of the compression molded samples was observed by atomic force microscopy (AFM) and the shift from two-phase to three-phase system was assigned to be responsible for the decrease of NIS at HDPE content great than 10 wt%.

Jang et al. reported a similar phenomena in IPC/HDPE blends at HDPE content of 0~20 wt%.[7] The NIS increased at low HDPE content (5~10 wt%) and decreased at HDPE content higher than 10 wt%. The authors explained this results by the separation of the HDPE from the EPR domains as a separated dispersed phase. In Jang et al.'s work, the morphology of the cross-section of the injection-molded tensile bar was observed by TEM but the morphology of the surface perpendicular the cross section was not shown.

Stehling et al. studied the structure and properties of PP/rubber/HDPE blends.[2] The influence of mixing sequence and HDPE content on the mechanical properties was reported. It is found that the impact strength increased when HDPE content increased from 6 to 12 wt%. The samples were microtomed,

xylene-etched and observed by SEM. Although the impact strength was tested using injection-molded samples, only the SEM micrographs of the compression-molded samples were shown.

Tchomakov et al. found that the morphology depends on PE viscosity and the mixing sequence for PP/PE/ethylene-propylene-diene (EPDM) blends and the mechanical properties changes correspondingly.[6] The dependence of NIS on PE content was found to be similar to the results of the work by Mirabella and Jang et al.'s. The NIS shows a maximum at PE content of 10 wt% for both of the PE resins with different melt index (MI, 4.8 and 0.5 g/10min, respectively). The solution of $KMnO_4$ and acid was used to reveal the detail structure of the blends and the PP, rubber and PE can be clearly identified, but, similar with the situation mentioned above, only the surface perpendicular to the flow direction in the injection-molded samples was analysed.

The works listed above all studied the effects of the addition of HDPE on the impact strength of PP/rubber/HDPE blends and the morphology has been noticed to be an very important factor. But there are still some pities. First, the specimens used in impact strength test are usually injection-molded and thus the morphology of the injection-molded specimens, rather than compression-molded ones, should be observed. Second, the injection-molding is known to induce an anisotropic structure.[13, 14] For this reason, the microtome should be conducted both perpendicular and parallel to the flow direction of the melt.

The role of the HDPE in influencing the mechanical properties of the PP/rubber/HDPE blends is also widely noticed. It is generally accepted that the morphology change induced by the addition of HDPE is an very important factor. A core-shell like structure has been reported by many researchers.[2-4, 6, 7, 11] The detail morphology of the particles composed by rubber and HDPE is varied, but in most cases, the rubber acts as "shell" and encapsulates the HDPE. Based on the core-shell structure, Gahleitner et al. stated that the addition of HDPE increases the "total elastomer volume" of a heterophasic copolymer and thus improves the NIS at room temperature to some extent.[3]

In this work, to elucidate the influence of HDPE on the morphology and the mechanical properties, two kinds of HDPE resins with different molecular weights were used to be blended with the IPC. The HDPE resins were blended with a IPC by HDPE content (w_{PE}) up to 40% based on total mixture weight. The specimens used in both of the mechanical property and morphology tests were injection-molded bars, which makes the relationship between the structure and the property more reliable. To study this kind of structure, the morphology of the plane both parallel and perpendicular the flow direction of the melt was observed. The morphology of the resulting blends was found to depend greatly on the molecular weight of the PE resins and the PE content and the mechanical properties changed correspondingly. Some results are different from the reported work. The relationship between structure and properties is discussed.

Experimental section

Materials. The impact polypropylene copolymer (IPC) resin is commercial product supplied by SINOPEC. The IPC is composed of isotactic polypropylene and ethylene-propylene rubber (EPR). The polyethylene (PE) samples used here are both commercial HDPE resins supplied by SINOPEC denoted by PE-A and PE-B, respectively. As shown in Table 1, the two PE resins have a great difference in molecular weights.

Xylene soluble fraction CrystEX made by Polymer Char company was used to obtain the xylene soluble (mainly EPR in the case of this paper) fraction (ω_{sol}) and the weight fraction of ethylene comonomer in soluble fraction (C2 in EPR). The CrystEX is equipped with a special IR sensor for ethylene content determination. The solvent is xylene. The value of ω_{sol} and C2 in EPR thus obtained are 29.25% and 39.53%, respectively.

Molecular weight and molecular weight distribution The gel permeating chromatography (GPC, PL-GPC220, Polymer Laboratories, Inc., Great Britain) and IRS detector (Polymer Char Inc., Spain) are used to measure the molecular weight and molecular weight distribution of the samples. The chromatography columns are three Plgel 10 μm MIXED-B columns connected in series, the solvent and fluid phase is 1,2,4-trichlorobenzene (comprising 0.3 g/1000 mL antioxidant 2,6-dibutyl p-cresol), the

column temperature is 150 °C, and the flow rate is 1.0 mL/min. We used a method set up by our laboratory to analyse the 1,2,4-trichlorobenzene soluble fraction in the IPC sample, which contains dissolving, filtration and GPC experiments. Molecular weight, molecular weight distribution can be readily obtained as well as the relative content of the soluble fraction. The parameters of the insoluble fraction can be obtained by subtraction of the result of soluble fraction from that of the IPC. Weight-average molecular weights (M_w) of the samples are shown in **Table 1**.

Table 1 Characteristics of the samples

	M_w	M_{cr}	$E_\eta(\infty)$	η_0 at 200°C[c]
	×10^3	g/mol	kJ/mol	Ns/m^2
IPC	301	/	/	/
Soluble fraction	614	5616[a]	38[a]	2.90×10^6
Insoluble fraction	227	7000[b]	43[b]	6.25×10^4
PE-A	222	3500[b]	27[b]	2.43×10^5
PE-B	87	3500[b]	27[b]	1.00×10^4

[a] Calculated by the C2 in EPR data and the corresponding data for PP and PE.

[b] Use the data in the handbook.[15]

[c] Calculated by equation (4)-(6) and the data in the handbook.[15]

Blend preparation. IPC and HDPE pellets were first mixed by a mechanical mixer. Then the mixed pellets were melted, blended, extruded and pelletized by ZSK-25 twin-screw extruder with a barrel temperature of 204-211 ºC. A compounded antioxidant of 0.3% by weight was added to supress the thermal decomposition during melt processing. The antioxidant is a mixture of Irganox 1010 and Irganox 168 with a ratio of 1:1 by weight. The pellets made thereof were dried at 80°C for at least 4 h before injection-molding to desirable specimens. The composition and the code of the blends are shown in Table 2, wherein the PE content denotes the weight content based on the total weight of the IPC and the HDPE.

Table 2 Basic formulations of the IPC/HDPE blends

Sample	HDPE type	HDPE content[a]	HDPE content[b]	Log(η_0)[c]	λ	D_n	D_w
		wt%	wt%	Ns/m^2		μm	μm
IPC	/	0	0	/	46.24	1.17	1.31
A1	PE-A	5.0	0.15	6.30	31.68	1.37	1.58
A2	PE-A	11.5	0.31	6.13	21.56	1.42	1.62
A3	PE-A	20.6	0.47	5.95	14.41	1.39	1.72
A4	PE-A	30.0	0.59	5.82	10.59	1.75	1.99
A5	PE-A	40.0	0.70	5.71	8.25	1.19[d]	1.49
B1	PE-B	5.0	0.15	6.09	19.49	1.61	1.83
B2	PE-B	11.5	0.31	5.70	8.09	0.91	1.07
B3	PE-B	20.6	0.47	5.30	3.22	0.75[e]	0.94
B4	PE-B	30.0	0.59	5.00	1.59	0.75[e]	1.02
B5	PE-B	40.0	0.70	4.75	0.90	0.88[e]	1.53

[a] HDPE content in the whole blends of PP/EPR/PE.

[b] HDPE content taken EPR/PE as a whole.

[c] Calculated by equation (7) and the data in **Table 1**.

[d] The length of the minor axis of the ellipsoidal particles of A5;

[e] The width of the oriented strips.

Measurement of Mechanical Properties. The specimens used for mechanical tests were injection-molded using the MA1200/370 injection-molding machine. The barrel temperatures of the injection-molding machine were 200 °C, respectively. The notched Izod impact strength （NIS）of the specimens was measured according to ISO180 at 20 ºC and -20 ºC. The tensile test was measured according to ISO527. For each sample, several parallel measurements were carried out and the average values were recorded.

Morphology. Morphology studies of the phase structure were done by scanning electron microscope Hitachi S-4800 for etched samples and FEI XL30 for fractured surface of samples after impact test. The specimens for SEM observation were cut from injection-molded bars for Izod impact tests and the observation area was the core of the bar. Due to the anisotropic characteristics of the injection-molded bar, it is necessary to mark different directions according to the flow direction and the geometry of the mold. The definition of the directions of the injection-molded bar is designated in Fig. 1. The specimens were cryomicrotomed in the presence of liquid nitrogen, etched by permanganic reagent according to Olley and Bassett's method[16], sputtered with gold and finally subjected to SEM observation. The morphology of the planes both parallel (XZ plane, as shown in Fig.1) and perpendicular (YZ plane, as shown in Fig.1) to the flow direction of the melt (X direction, denoted as FD) were revealed by microtome. Thus the flow-induced morphology can be readily observed.

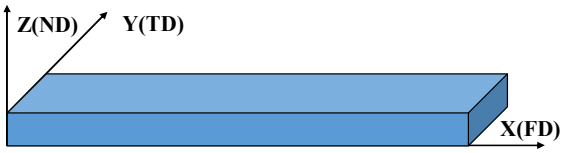

Fig.1 Definition of the direction, X is the flow direction denoted as FD, Y is the transverse direction denoted as TD and Z is the normal direction denoted as ND.

The size of the dispersed phase was evaluated by the **Nano Measurer** software programmed by Ms Xu Jie in the department of surface chemistry and catalysis laboratory in Fudan university. For spherical particles, number (D_n) and weight (D_w) average particle diameter were measured and calculated by equation (a)[17]. For spherical particles, diameter was measured directly, for oriented dispersed phase, the width, i.e. the shorter dimension was measured, which is also denoted as D_n and D_w.

$$D_n = \frac{\sum_{i=1}^{N} n_i D_i}{\sum_{i=1}^{N} n_i} \quad , \quad D_w = \frac{\sum_{i=1}^{N} n_i D_i^2}{\sum_{i=1}^{N} n_i D_i} \qquad (1)$$

Results

Morphology

Permanganic etching has been proved to be effective in characterization of semi-crystalline polyolefins, combined with proper specimen preparation methods such as cryo-microtome and observation methods such as SEM and TEM.[6, 16, 18-21] It is found that the etchant is capable to discriminate different components in multi-phase system as complicated as the in-reactor alloy. Fine structure at lamellar level can be revealed as the etchant selectively removes defective regions.[18]

With the aid of the permanganic etching method, the morphology of the dispersed particles composed of EPR and HDPE can be clearly observed, which is schematic in **Fig.2**. In **Fig.2**, the PE part is represented by light grey and the EPR dark grey. Basically, all of the particles observed in this study own an overall core-shell like structure, wherein the EPR acts as the shell and PE the core. Based on the shape and amount of the PE, five kinds of particles were observed, which were denoted as type I~V.

The characteristic of type I particle is that this kind of particles contain one PE inclusion in the EPR domain and the EPR is the majority part. In type II particles, there are several PE inclusions in one EPR domain and the EPR is still the majority part. In type III particles, the core consisting of PE is large and acts as the majority part and the EPR layer encapsulating the PE is very thin. Type IV particles contain several PE inclusions and the inclusions is the majority part. Type V particles also have an overall core–shell structure and the large PE core is encapsulated by EPR shell. The shape of the PE core is somewhat irregular. Some EPR particles are included in the PE domain and some EPR penetrate into the PE domain through the EPR/PE interphase, as shown in **Fig. 2**.

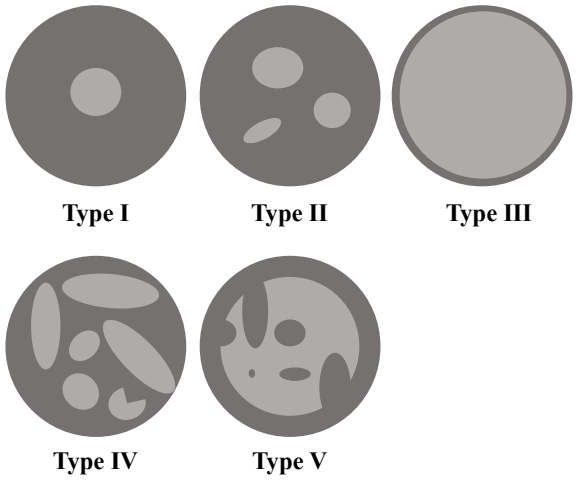

Fig. 2 Illustration of the composite particle composed of EPR and PE. The darker part represents EPR and the lighter part crystalline PE.

Morphology of IPC The morphology of the IPC sample used in this study is typical of in-reactor alloy as shown in **Fig.3 (a)~(b)**. **Fig.3 (a)** and **(b)** is the morphology of the YZ and XZ plane (see **Fig.1**) of the injection-molded sample, respectively. In the SEM pictures, the dispersed particles can be clearly seen. In many particles, PE-type inclusions with lighter color can be identified. As shown in **Fig.3** (a) and (b), when observed along X (YZ plane) and Y (XZ plane) direction, the EPR rubber particles dispersed in PP matrix both appear to be nearly round and no apparent difference was observed. This indicates that there is no anisotropic structure in the observed section of the IPC injection-molded bar and the dispersed EPR phase owns a nearly spherical shape. Inside some EPR particles, there are one or more “inclusions”, which are assigned to PE-type crystalline fractions[3, 4] and can be represented by type I and II particles as shown in **Fig. 2**, respectively.

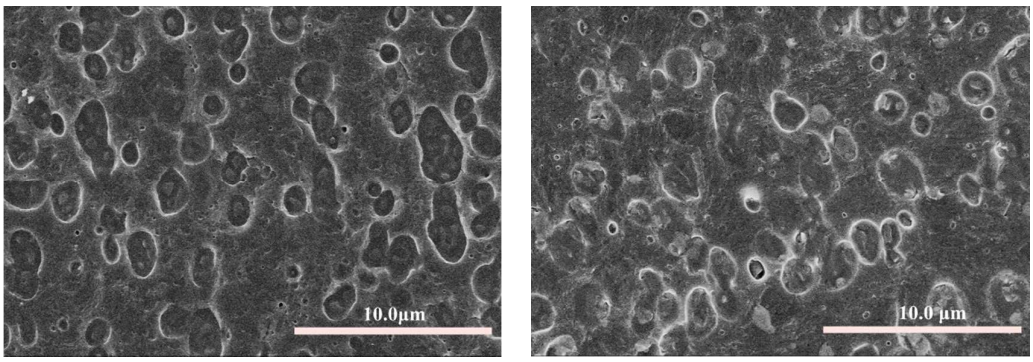

(a) (b)

Fig. 3 SEM micrographs of IPC. (a) YZ plane and (b) XZ plane as shown in **Fig.1**, Z is horizontal.

The SEM pictures of the XZ plane for the blends with different type and amount of PE are shown in **Fig. 4 and 5** and pictures with larger magnification for A 5 and B1 are also shown in **Fig. 6 (a) and (b)**, respectively. The SEM picturesof the YZ plane for A3 and B3 are shown in **Fig. 7 (a) and (b)**, respectively. In the SEM pictures, components can be identified by the color contrast combined with the interface between the different phases. PE appears lighter, PP and EPR darker. Furthermor, the lamellae of the crystalline PE can be clearly revealed as shown in **Fig. 6 (a)**.

The SEM micrographs of the XZ plane for blends A1~A5 are shown in **Fig. 4 (a)-(e)** and those of the YZ plane are shown in **Fig. 7**(a) for A3 and **SFig.1** (a) and (b) (see supporting information) for A2 and A3, respectively. It is found that the dispersed particles are all nearly round in shape for both XZ and YZ plane. This situation is the same as that in IPC, which indicates that the dispersed phase in A2 and A3 are spherical particles and it also can be concluded from **Fig.4** (a) and (d) that the dispersed phase in A1 and A4 are also spherical. The orientation in the A5 can clearly shown by XZ plane morphology as shown in **Fig.4** (e).

As shown in **Fig. 4** and SEM micrographs with higher magnification (**Fig.7(a)**), the structure of the dispersed phase for A1-A5 can be identified. The core-shell structure can be found in all the five samples but the detail structure of the composite particles is greatly influenced by the w_{PE}. For A1 sample with low w_{PE} (5 wt%), as shown in **Fig. 4(a)**, type I and II particles are found, which is similar with the IPC. Due to the addition of PE, more PE is included in EPR particles and thus type III morphology is also found in A1. When w_{PE} increases to 11.5%, as shown in **Fig. 4(b)**, an obvious change in morphology occurs. EPR particles, type I and type II particles are rarely seen. There are mainly type III and type IV particles. When w_{PE} increases to 20.6% and 30%, as shown in **Fig. 4(c) and (d)**, type III, IV and V particles dominate. The type V particles may evolve from type IV during the coalescence of the PE particles in the EPR domain. When w_{PE} increase, the separated PE particles existing in the same dispersed composite particles begin to coalesce and the EPR phase should be pushed out. But some EPR particles are "frozen" in the PE domain due to kinetic reason, for which the EPR has no enough time to be pushed out of the PE domain before solidification of the system. For A5, in which the w_{PE} is as high as 40wt%, the PE content is nearly the same with the PP content. But the PE/EPR composite particles still exist and act as dispersed phase, which are also core-shell type. Round and oriented particles along the FD can both be found in A5, as shown in **Fig.4 (e)**, which is different from A1~A4 to some extent. An aspect ratio as high as 7 is found in the oriented particles. Accordingly, orientation of the PE crystallites takes place in such kind of particles, as shown in **Fig.6 (a)** at higher magnification, where the existence and orientation of the lamellae of crystalline PE can be clearly seen. The layer normal of the lamellae have a preferred orientation along FD direction.

As shown in **Table 2**, the D_n of IPC and A1-A4 increases from 1.17 to 1.75 μm with the addition of PE. This indicates that when the w_{PE} increases, more PE is encapsulated in the dispersed phase, which leads to a increase in the volume fraction of the dispersed phase and complexity of the particles. Consequently, the particle size increases and the interdistance between the particles decreases. But due to the compatible

effect of the EPR in PP/EPR/HDPE blends[3, 4], the size and shape of the particles do not change too much and the aggregation of the particles is also limited. When w_{PE} increases further to 40 wt% (A5), a relatively great change in the morphology takes place. Some particles are no longer spherical and a preferred orientation along FD is found but the PE/EPR composite particles still act as dispersed phase.

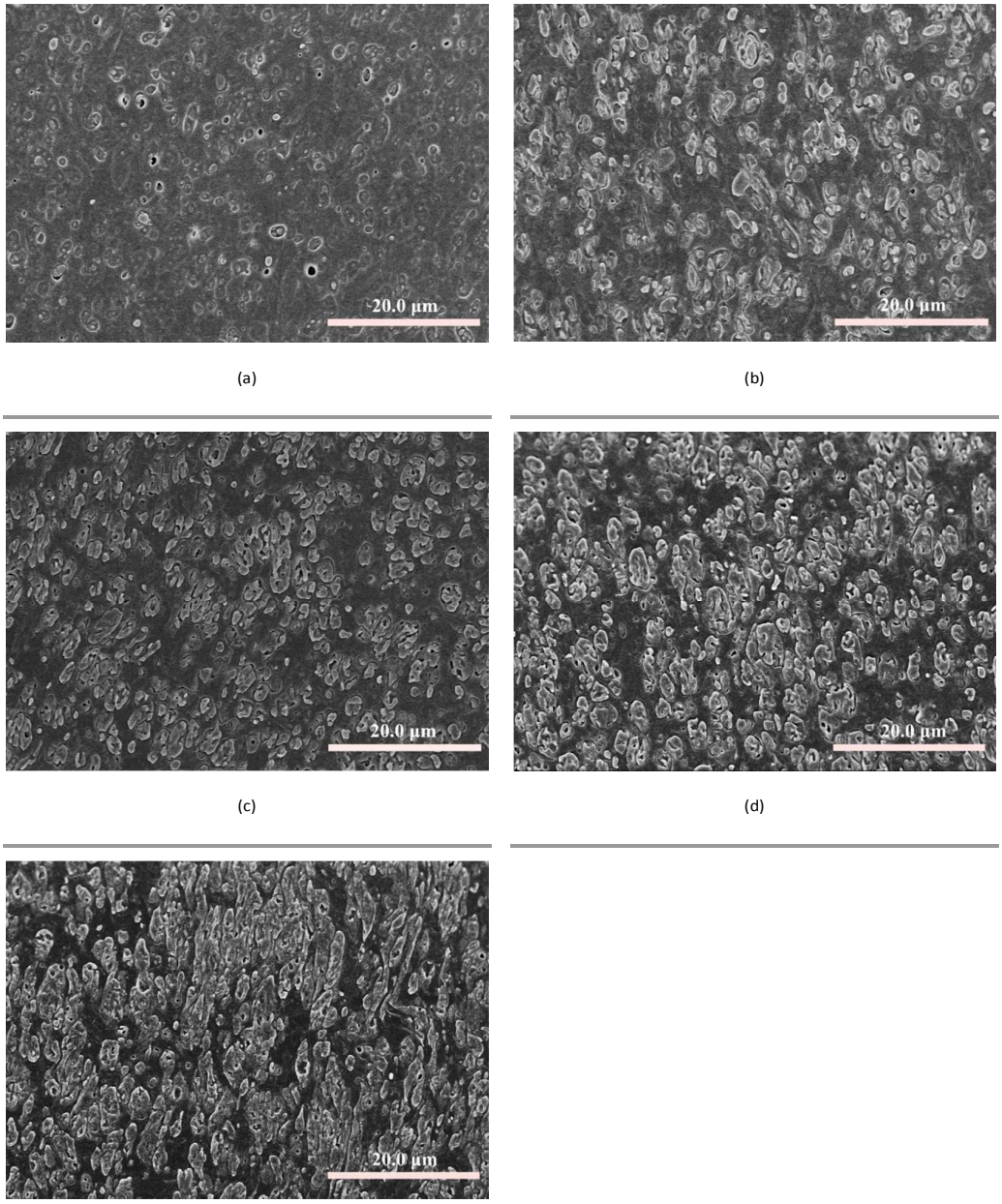

Fig. 4 SEM micrographs of the XZ plane of the A1~A5 sample. (a)~(e) are corresponded to A1~A5 samples, respectively. Z is horizontal.

For blends B1~B5, which contain low molecular weight PE, the situation becomes quite different, as shown in **Fig.5 (a)~(e)**. In the SEM micrographs of XZ plane of B1 and B2, as shown in **Fig.5 (a)** and **(b)**, the dispersed phase show a round shape. But for B3-B5, highly oriented morphology can be identified. Combining with the SEM micrographs of YZ plane for B2 and B3, as shown in **SFig.1** (c) (see in supporting information), **Fig.7** (b) and **SFig**.1 (d) (see in supporting information), respectively, it is clear that dispersed phase in B2 is mainly spherical particles as IPC and A1-A4 and dispersed phase in B3 is

strip-like. The morphology of B1 can be concluded to be similar as that in B2, and B4 and B5 as that in B3. That is to say, the morphology of B1 and B2 is essentially the same with that of A1, in which spherical particles with the EPR shell and PE core can be clearly identified, as shown in **Fig. 6(b)**. The orientation of the dispersed phase along FD direction becomes very obvious when w_{PE} equals to and/or exceeds 20.6 %, as shown in **Fig. 5 (c)~(e)**. For B3 and B4, "long strips" composed of PE and EPR were observed, which had a width as low as 0.2~1.6 μm and a length as high as tens of microns. When w_{PE} is as high as 40% (B5), the orientation of the PP domain and the PE/EPR domain is very obvious.

Then the dimension of the PE/EPR phase in B1-B5 is to be considered. The data is listed in **Table. 2**. For B1 and B2, in which spherical particles exist, different particle sizes are found. For B1, D_n is 1.61 μm, which is larger than that of IPC due to the increase of overall volume fraction of the dispersed phase. But D_n becomes 0.91 μm for B2 at w_{PE} = 11.5 wt%, which is smaller than that of IPC, A1-A5 and B1. This may due to the decrease of the viscosity of the dispersed phase, which will be discussed in the following part of this paper. The width of the strips, which can represent the diameter of the cross-section of the strips (also denoted as D_n here), in B3-B5 is measured and is listed in **Table.2**. Due to the elongation effect, the D_n values for B3-B5 is apparently smaller than that in the counter part with same PE content in A3-A5. The D_n value is larger and the spacing between the strips seems lower in B3 than those in B3 and B4 because of the higher w_{PE} in B5, in which the w_{PE} is similar to PP content.

The morphology of YZ plane of A3 and B3 is compared as shown in **Fig.7** (a) and (b), respectively. There are 91 particles in **Fig.7** (a) and 166 particles in **Fig.7** (b) and the D_n is 1.16 and 0.65μm, respectively. Assuming the particles seen in the SEM micrographs are all perfectly round, the area occupied by dispersed phase for A3 and B3 is 96.1 and 55.1 μm^2, respectively. Considering the volume fraction of the dispersed phase is the same for A3 and B3, it can be concluded that more material is distributed in the X direction because of the long strip morphology in B3. But the count of the particles is higher in B3, so the particles in **B3** appears to be denser. This furtherly confirms that, when the dispersed phase particles are spherical, the apparent size of the particles in YZ plane is apparently larger than that in samples with oriented dispersed phase and the number of the particles is lower. Such kind of morphology difference appears to have a great influence on the toughness and elongation behaviour of the materials, which will be discussed in the following part in this paper.

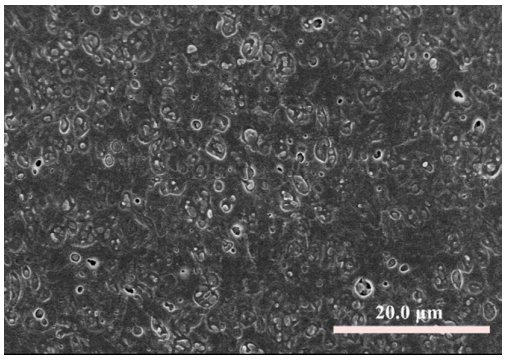

(a)

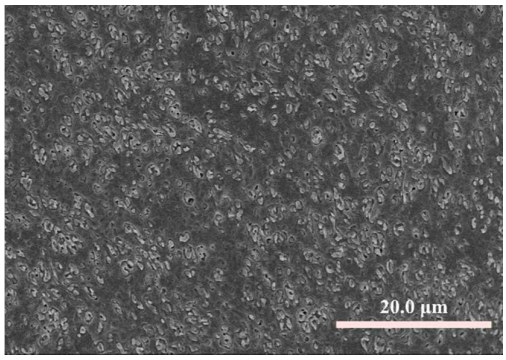

(b)

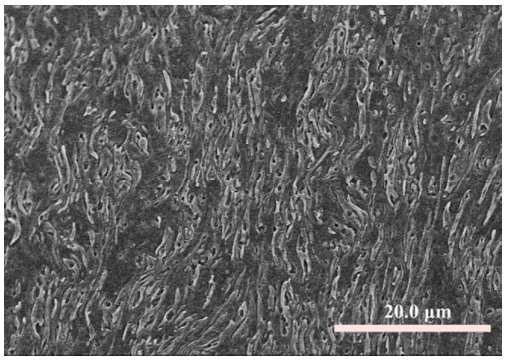

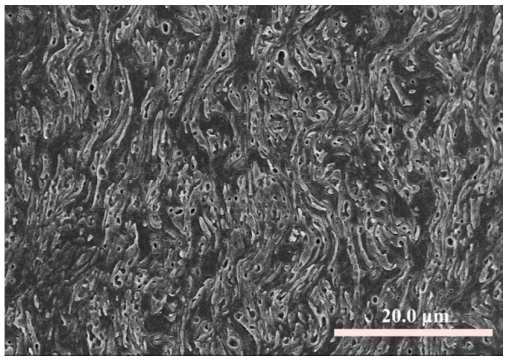

(c) (d)

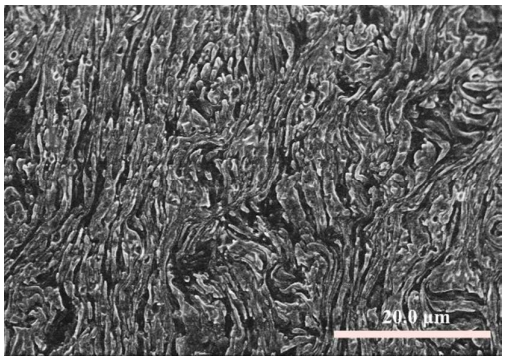

(e)

Fig. 5 SEM micrographs of the XZ plane of the B1~B5 sample. (a)~(e) are corresponded to A1~A5 samples, respectively. Z is horizontal.

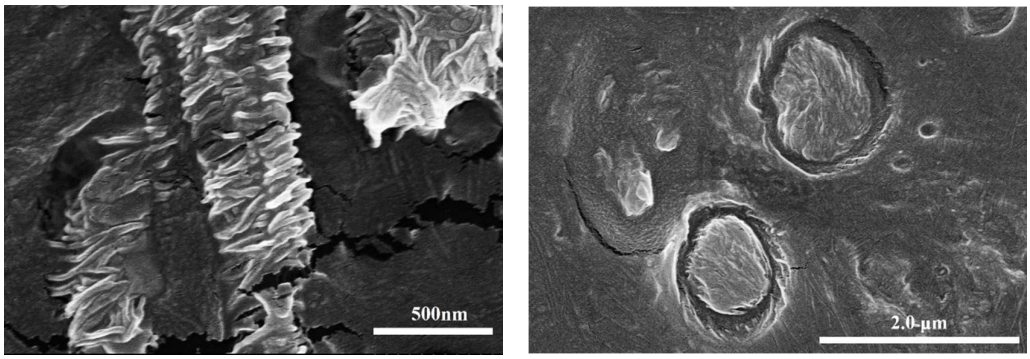

(a) (b)

Fig. 6 SEM micrographs of the XZ plane of A5 (a) and B1 (b) samples, respectively. Z is horizontal.

From the results shown above, it is found that the morphology of the blends is greatly effected by the type and molecular weight of the PE added. The morphology in turn affects the mechanical properties, which will be discussed in the following section.

It is also important to remind that the study in the samples prepared by methods which may induce orientation such as injection-molding, extrusion etc. should be conducted with care. Taking the results in this paper for example, misleading may occur when only the morphology of YZ plane is to be considered, which is the common situation because the cryo-fracture of the injection-molded bar is easy to realise. For B3-B5 samples in this paper, the morphology of the YZ plane as shown in **SFig.1(d)** (supporting information) and **Fig.7** (b) is not enough to reveal the real morphology. Thus the observation of YZ plane is necessary and the existence of oriented morphology can be more effectively observed by YZ plane view.

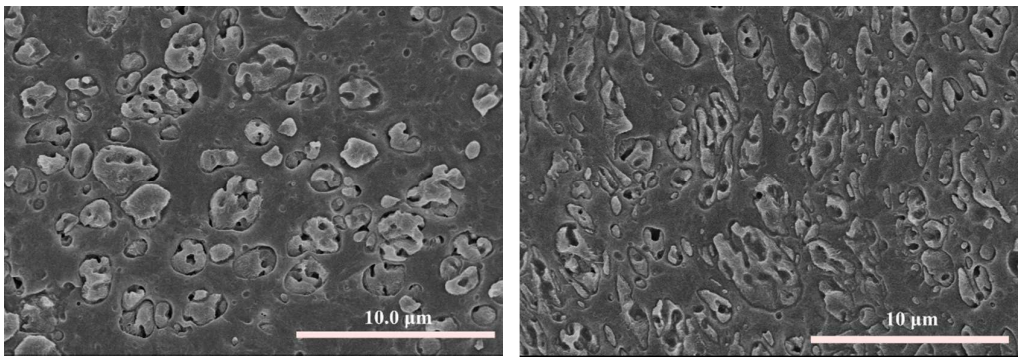

Fig. 7 SEM micrographs of the YZ plane of A3 (a) and B3 (b), respectively. Z is horizontal.

Mechanical Performance

Notched Izod impact strength (NIS) of the IPC and blends at room temperature and -20ºC is plotted against PE content in **Fig. 8**. For IPC and blend A1~A5, at room temperature, NIS increases with increasing PE content at 0~20.6 wt% and levels off with further increase of w_{PE} up to 40wt%. The situation is similar for NIS at -20ºC.

For blend B1~B5, at room temperature, NIS of B1 slightly increases compared with that of IPC and afterwards, NIS of B2~B5 decreases upon the increase of PE content. When w_{PE} is greater than 20.6%, the NIS of the blend is lower than that of the IPC. The trend of NIS at -20ºC is similar to that at room temperature. NIS of B1 is greater than that of the IPC and then NIS goes downwards. At w_{PE} greater than 20.6 wt%, NIS is lower than that of IPC, but NIS of B5 increases slightly with respect to B3~B4 and is still lower than that of the IPC.

The elongation at break (ε_b) was also found to have a tight relationship with morphology. As shown in **Fig. 9**, elongation at break of A1 (245%) is nearly four times of that of IPC (63%) and ε_b decreases with further increase of w_{PE}. The ε_b reaches to a minimum of 25% at w_{PE}=20.6% and then slightly increase to 31% (A4) and 53% (A5). The ε_b of B1 and B2 is nearly the same with that of the IPC and ε_b has a increase from 33 (B2) to 260% (B3) at the w_{PE} of 20.6 %. Further increase of ε_b takes place when w_{PE} increases from 20 to 40%. ε_b as high as about 460% was found at w_{PE}=40%. It is obvious that the orientation morphology in B3~B5 plays an important role in increasing the ε_b.

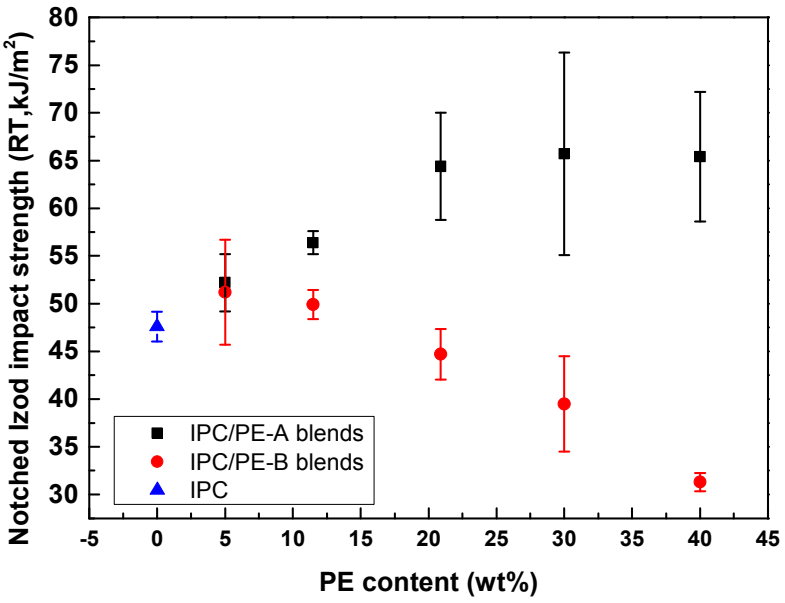

(a)

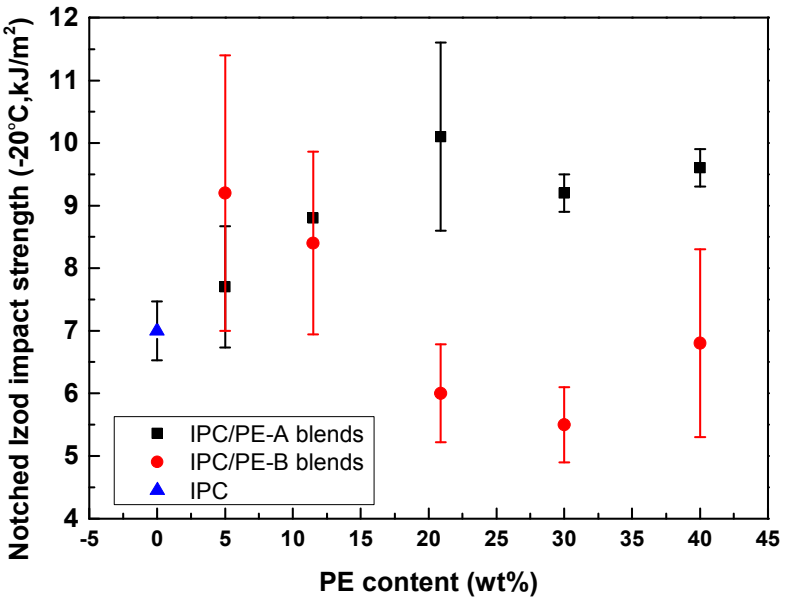

(b)

Fig. 8 Notched Izod impact strength of IPC and the IPC/PE blends. (a) room temperature, (b) -20 ºC. (error bar is added)

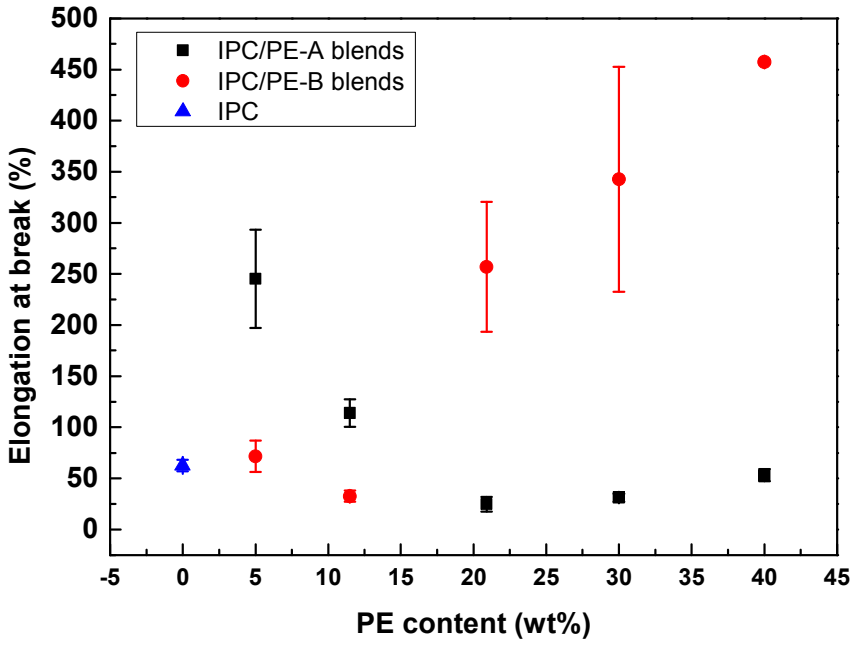

Fig. 9 Elongation at break of IPC and IPC/PE blends. (error bar is added)

Discussion

Influence of PE content and molecular weight on morphology

It can be concluded from the observation above that the molecular weight and amount of PE both have a significant influence on the morphology of the injection-molded specimens. Decreasing the molecular weight of PE and increasing the PE content all contribute to the formation of the orientation structure. For B1~B5, orientation begins to occur at w_{PE} =11.5% and becomes very obvious at w_{PE} ≥20.6%. For A1~A5 samples, which contain higher molecular weight PE, oriented morphology was observed only at w_{PE} =40% and the orientation degree is relatively less pronounced compared with that in B3~B5.

Then it is shown to be very important to discuss the factors influencing the morphology. The phase structure of the PP/EPR/PE heterophasic system is determined mainly by three factors: viscosity ratio between the dispersed and the matrix phase (λ), compatibility between components and conditions of compounding and processing.[3] In the system studied in his paper, the PP and EPR are the same (the same IPC) and the difference of the PE is only molecular weight. The compounding and processing is also the same for all the samples. So the viscosity ratio seems to be the key factor. The importance of the viscosity ratio in determining the morphology IPCs has been reported by many researchers.[3, 22-26] The viscosity ratio (λ) and the capillary number (κ) are defined below:[22]

$$\lambda=\eta_d/\eta_m \quad (2)$$

$$\kappa=\eta_m \dot{Y}/(v/D) \quad (3)$$

where η_d and η_m are the viscosity of dispersed and continuous phases, respectively and $\dot{Y}$, v, and D are the shear rate, interfacial tension, and droplet diameter, respectively. The deformation of the dispersed phase is reported to be determined by λ and κ. Critical values are reported for different polymer blends such PP/EPR[22, 27], PP/PE/EPR[22] and PE/PS[28] blends. λ being close to or less than unity seems to facilitate the formation of fibril morphology of the dispersion phase[22, 27-30] (corresponding to the oriented morphology mentioned in this paper).

Due to the difference in experiment conditions and samples selected, λ can be expressed by different forms in the literatures. It was reported to be obtained by measuring Brabender torque values[31], the ratio of zero shear viscosity (η_0)[32] and the ratio of intrinsic viscosity[25, 26].
In this work, we use IPC samples and thus it is difficult to measure the melt viscosity of the individual EPR and PP phase. But the molecular weights of the EPR (soluble fraction) , PP and PE can be readily measured by GPC, so the η_0 of the components at the injection-molded temperature T (here is 200°C) is calculated according to equation (4)-(6) below[15]:

$$\log\eta_{cr}(1.2T_g) = E_\eta(\infty)\left(\frac{0.052-8.5\times10^{-5}}{T_g}\right)-1.4 \quad \textbf{(4)}$$

$$\log\frac{\eta_{cr}(T)}{\eta_{cr}(1.2T_g)} = \frac{0.4343E_\eta(\infty)}{RT_g}\left(\frac{T_g}{T}-1\right) \quad \textbf{(5)}$$

$$\log\eta_0(T) = \log\eta_{cr}(T)+n\log\left(\frac{M_w}{M_{cr}}\right) \quad \textbf{(6)}$$

T_g is the glass transition temperature, $E_\eta(\infty)$ is the value of activation energy for viscous flow (E_η) for T>>Tg (glass transition temperature) , which can be calculated by the additive function[15], η_{cr} is the viscosity at critical molecular weight. M_w is the weight average molecular weight, M_{cr} is the critical molecular weight. n is determined by M_w of the samples. In the case in this paper, n is 3.4 because the M_w of the PP, PE and EPR used here are all greater than the critical values (M_{cr}).[15] Tg value of the PP and PE can be found in handbook[15] and Tg of EPR is obtained by DMA (TA RSA-III), which is -52.5°C (see **SFig.2** in the supporting information). The parameters for EPR such as M_{cr} and $E_\eta(\infty)$ are estimated by the values of PP and PE combining with the weight fraction of ethylene in EPR (C2 in EPR). The η_0(200°C) values of soluble fraction (mainly EPR), insoluble fraction (mainly PP) thus calculated are listed in **Table 1**.

The molecular weight of the dispersion phase consists of PE and EPR, thus the melt viscosity of the PE/EPR blends, as a whole, is the key factor influencing the morphology. The viscosity of the blends obeys the logarithm mixing rule:[24, 33, 34]

$$\log\eta = \omega_1\log\eta_1 + \omega_2\log\eta_2 \quad \textbf{(7)}$$

where η is the viscosity of the blend, η_1 and η_2 are the viscosities of the two components measured at the same temperature, respectively, ω_1 and ω_2 are the volume fraction of the components. The η_0(200°C) values of the EPR/PE, as a whole are listed in **Table 2** and the viscosity ratio values between EPR/PE phase and PP phase are also given in **Table 2** and plotted in **Fig.10**. For IPC, the viscosity ratio is obtained by η_0(200°C) value of EPR and PP.

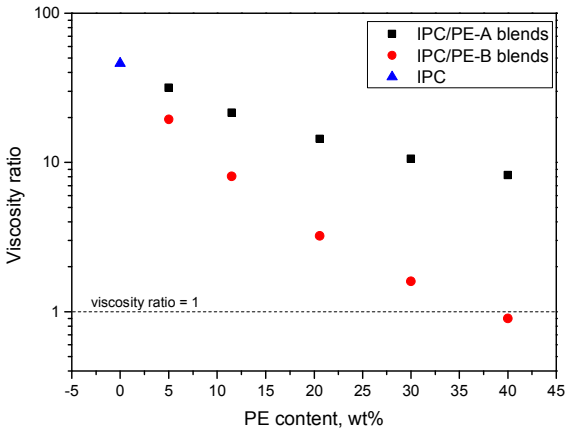

Fig. 10 Viscosity ratio for IPC, IPC/PE-A and IPC/PE-B blends.

From **Fig.10,** it is obvious seen that the difference in molecular weight and blending content of PE leads to a change in viscosity ratio between the dispersed phase consisting of PE and EPR (or EPR for IPC) and matrix (PP). In this study, the molecular weights of the two PE samples are both lower than that of the EPR (soluble fraction of the IPC as shown in **Table 1**), thus the addition of PE lowers the viscosity of the PE/EPR composite phase. But the degree of the decrease in the viscosity of the dispersed phase varied for different PE molecular weight and content. When PE is mixed with EPR by higher fraction or PE with lower molecular weight (PE-B) is used, the decrease of viscosity ratio is much more severe. According to the results reported by the literatures[22, 28, 29], the lower the viscosity ratio ($\lambda \leq 1$), the easier the oriented fibre-type dispersed phase to occur under shear flow. For B1-B5 blends, according to SEM results, the orientation of dispersed phase occurs at w_{PE} =20.6%, where the viscosity ratio is 3.22. At PE content = 40%, viscosity ratio is as low as 0.90. For A1-A5 blends, the viscosity ratio ranges from 8.25-31.68, which is much higher than those of B1-B5. Thus it is much harder for the A1-A5 blends to form the oriented dispersed phase.

From the analysis above, it can be concluded that the formation of the oriented structure can be attributed to the decrease of viscosity of the dispersed phase due to the increase of PE content and/or the lower PE viscosity. It should be noticed that orientation can be observed in A5, but it is not as obvious as that in B3~B5. The viscosity ratio is 8.25 for A5, which is higher than that of B3. It may be inferred that it is easier for the formation of the oriented structure when the PE content is high enough, in which case the weight contents of the PP and PE are close to each other.

It should also be emphasis that during the processing in the twin-screw extruder and injection-molding, the polymer melt undergoes a complex flow, in which multi modes of deformation may exist such as shearing, extension etc. So the viscosity in the real processing condition is complex but it is beyond the scope of this paper.

Influence of the morphology on the mechanical properties

The addition of PE is believed to increase the overall volume of the elastomer particles and thus lead to an increase in NIS.[3, 7, 12] It has been reported that there exists an maximum at a w_{PE} of about 10 wt% in the NIS versus PE content curve of IPC/HDPE blends at room temperature [7, 11]. Gahleitner et al.[3] reported that the NIS of a random-heterophasic copolymer/HDPE increases with increasing PE content at PE content of 0~15 wt% and change little from 20 to 25 wt% at 23ºC, but at -20ºC, NIS goes down monotonically. In this work, for the two series of blends with different PE, the change of NIS with respect to PE content depends greatly on the type of PE added both at room temperature and -20 ºC and distinct trends were found. It can be found that the NIS has an obvious relationship with the morphology.

For blends A1~A4, when the PE content increases from 5 to 30 wt%, the dispersed phase keeps a nearly spherical shape and even at 40 wt% (A5), the orientation of the dispersion particles is still not very obvious. This indicates that if the dispersion particles remain a nearly spherical shape, the addition of PE plays a role in increasing the "total elastomer volume"[3] and thus leads to an increase in NIS at both room temperature and -20 ºC. But when PE content exceeds 20.6 wt%, the increase of NIS at room temperature and -20 ºC is very little. This indicates that the detail structure of the composite particles (such as type IV and V particles) and relatively low degree of orientation of the particles have no obvious influence on the NIS. This also indicates that the particle size (D_n) has little effect on NIS for A3 and A4, where the D_n change from 1.39 to 1.75μm.

For B1~B5, the maximum of NIS locates at the PE content of 5% at both temperatures. For blend B1 and B2, the particles are predominantly spherical and thus the NIS of them is larger than that of IPC at both temperatures. It is at the PE content of 20.6% that the NIS begins to become lower than that of IPC at both temperatures and it should be emphasized that the apparent morphology change also takes place at this PE content. This means that it is the oriented strip-like morphology which leads to a decrease in the NIS. That is to say, when oriented morphology occurs, the further addition of PE will cause a decrease in NIS.

Compare the NIS of A series sample (NIS_A) with those of B series (NIS_B), it is found that the A samples are much tougher than B samples at PE content greater than 5wt% both at room temperature and -20ºC. This indicates that the spherical particles are more effective in toughening the material. At PE content of 5wt%. NIS_A is nearly the same with NIS_B at room temperature and the NIS_B is higher at -20ºC because at PE content of 5wt%, the dispersed phase particles are all spherical for both A and B samples.

The negative effect of strip-like morphology can also be confirmed by the experiment result of crack surface observation for samples after NIS test. The morphology of the cracking surface (YZ plane) of A5 and B5 after impact test at -20 ºC was observed and the SEM micrographs are shown in **Fig.11 (a)** for A5 and **(b)** for B5. The difference in the morphology is obvious, that is, the surface of A5 is much coarser than of B5. For A5, a lot of granules and holes with a diameter of about 0.5 -1.6 μm can be found, but for B5, the amount of the granules and holes is much less than that in A5 and the size of them is also much smaller (about 0.4μm). Obviously, A5 with coarser surface owns higher toughness.

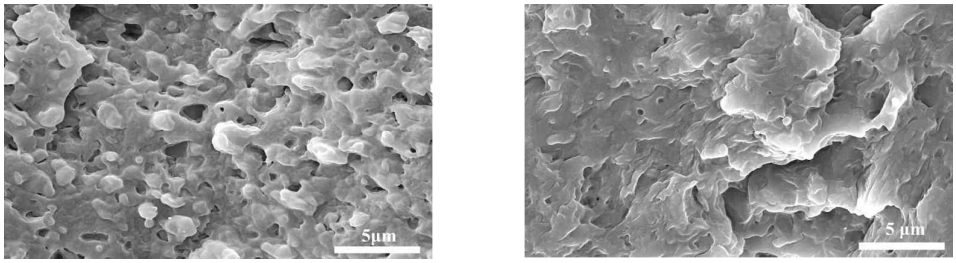

(a) (b)

Fig. 11 SEM micrographs of the cracking surfaces (YZ plane in **Fig.1**) of the A5 (a) and B5 (b) samples after NIS test at -20ºC.

Although the samples with oriented structure is inferior in toughness, the elongation at break is superior for this kind of samples. From **Fig.9**, it is obvious shown that, for B1-B5, the ε_b begins to increase rapidly at w_{PE}=11.5wt%, just at which w_{PE} point the strip-like morphology occurs and develops with further addition of PE. For A1-A5, in which the spherical particles or slightly oriented particles exist, ε_b increases for A1 compared with that of IPC and decreases from w_{PE} 5 to 20.6% and keeps nearly unchanged afterwards. The ε_b of B3~B5, in which strip-like morphology is observed, are greatly larger than those of A3~A5. Here, the role of the oriented morphology in the enhancement of ε_b is very pronounced. For A1~A2 and B1~B2, in which the particles are basically all spherical, the ε_b of A1~A2 is greater than those of B1~B2. This further proves the importance role of the orientation structure in the ε_b.

Why does the oriented morphology influence the mechanical properties so significantly? Undoubtedly, the anisotropic morphology of the injection-molded samples plays an important role. When the samples are subjected to impact or tensile tests, the force is imposed in the specific direction(s). Thus it is reasonable to conclude that the morphology of some specific plane(s) corresponding to the specific force is crucial in the mechanical properties. For convenience, this morphology of this plane is name as "effective morphology".

When the dispersed phase particles are spherical, the morphology of the XZ plane and YZ plane are basically the same, such as IPC shown in **Fig.3** (a), (b) and A3 shown in **Fig.4(c)** and **Fig.7(a)**. In this case, the morphology of the XZ and YZ plane can both be taken as "effective morphology". This is the generally seen morphology for impact copolymers, for which the fraction of the dispersed phase is dominant factor in determining the NIS.

When orientation morphology exists, the morphology of the XZ and YZ plane is distinct and it is reasonable to conclude that one of them is responsible for the decreased NIS and increased ε_b compared with those without oriented morphology. Taking the comparison of A3 versus B3 and A5 versus B5 as examples, the NIS of A3 and A5 is much larger than those of B3 and B5 both at room temperature and -20ºC, respectively, but the ε_b of A3 and A5 is much smaller than that of B3. As discussed above, considering the morphologies of YZ plane of A3 versus B3 and A5 versus B5 shown in **Fig.7 (a),(b)** and **Fig.11 (a),(b)**, respectively**,** compared with A3 and A5, the amount of particles is much larger and the particle size is much smaller in B3 and B5. According to toughening theory, in toughened crystalline plastics, the role of dispersed rubber phase is to initiate the craze and shearing yielding[35, 36] and it is reported that smaller particle size leads to higher toughness in impact polypropylene copolymer both for PP/EPR[37-39] and PP/EPR/HDPE[2] blends. From this point of view, it seems that the NIS of B3 should be larger than that of A3 and B5 larger than A5 but the situation is reversed here. From the experiment results in this work, it is shown that the morphology of XZ plane seems to the "effective morphology", which is the oriented strip-like morphology.

The influence of the effective morphology on the NIS is illustrated in **Fig.12**. For samples in which spherical or nearly spherical particles dominate (A1-A5 and B1-B2), the fracture happens in YZ plane and the detachment of the particles from the matrix happens in the NIS test, which induces the formation of granules and holes in the fractured surface as shown in **Fig.12 (a)** (the A type morphology) and SEM micrograph **Fig.11(a)**. For samples which own effective morphology as shown in **Fig 12 (b)** (B3-B5), when fracture happens, most strips are broken in the cross section and the B type morphology is observed (**Fig.12(b)**) but A type morphology is fewer, which results in a relatively smoother surface. The coarser fractured surface dissipates more impact energy and thus samples with spherical dispersed phase own higher NIS.

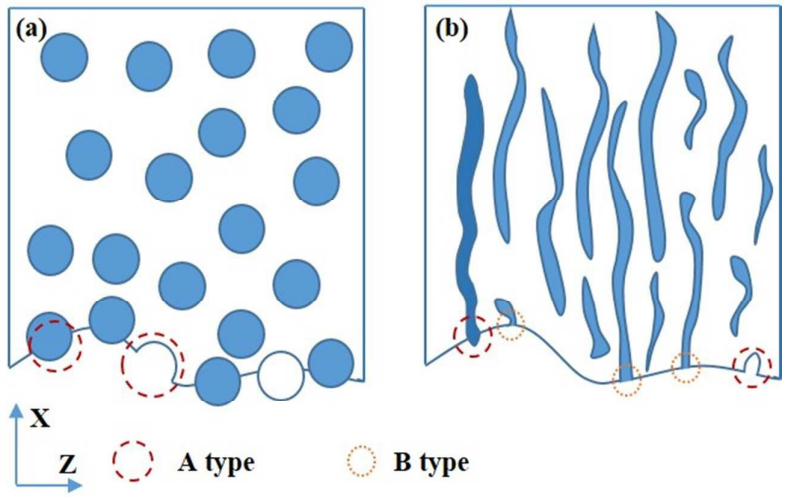

Fig. 12 Schematic illustration of the effective morphology (morphology of XZ plane) of the injection-molded bar.

The occurrence of the oriented strip-like morphology gives rise to ε_b. The influence of orientation morphology on ε_b seems more straight forward. In this work, the tensile force is along X (FD), which is in the same direction as the long axis of the strips composed of PE and EPR. When the samples were subjected to tensile deform, this kind of structure may not as easy to initiate the fracture as that when the particles are spherical and the existence of the oriented strip may also facilitates the mobility of the crystallites of iPP. The detail mechanism is worthy of a further study.

It is also meaningful to point out that, an interesting characteristic of the oriented structure is that it is an anisotropic system. It is anticipated that if the direction of impact or tension changed, distinct behaviour might be observed, which is worthy of further study.

Conclusions

From the experiment results and discussion above, it is found that the molecular weight and the content of PE both have great influence on the morphology and properties of the injection-molded products IPC/PE blends. The morphology can be tuned by adjusting the molecular weight and the content of the PE.

An important observation of this work is that the impact strength of the IPC/PE blends depends on not only on the PE content, but also on the morphology. “Effective morphology” is suggested to govern the properties. The dispersed particles are effective in toughening only when the particles is spherical or nearly spherical. The orientation of the dispersed phase has a great negative effect on the impact strength. When orientation exists, upon the increase of PE content, the impact strength decreases monotonically up to the limits in this work.

Although having negative influence on impact strength, the existence of the orientation structure of the dispersed phase greatly enhances the elongation at break values of the samples. There is an increase of above 600% of the elongation at break value when PE content is as high as 40wt%.

Acknowledgements

The author gratefully thank the SINOPEC Beijing Research Institute of Chemical Industry for the support of this work. The author also thank Xiaoguang Cai, Wenjun Wei, Honghong Huang, Dong Wei, Dan Wang, Yiqing Bai for the valuable discussions and the technical help.

Notes and references

1. C. Grein, K. Bernreitner, A. Hauer, M. Gahleitner and W. Neissl, *J. Appl. Polym. Sci.*, 2003, **87**, 1702-1712.
2. F. C. Stehling, T. Huff, C. S. Speed and G. Wissler, *J. Appl. Polym. Sci.*, 1981, **26**, 2693-2711.
3. M. Gahleitner, A. Hauer, K. Bernreitner and E. Ingolic, *Int. Polym. Process.*, 2002, 318-324.
4. M. Gahleitner, C. Tranninger and P. Doshev, *J. Appl. Polym. Sci.*, 2013, **130**, 3028-3037.
5. P. Galli, T. Simonazzi and D. D. Duca, *Acta Polymerica*, 1988, **39**, 81-90.
6. K. P. Tchomakov, B. D. Favis, M. A. Huneault, M. F. Champagne and F. Tofan, *The Canadian Journal of Chemical Engineering*, 2005, **83**, 300-309.
7. H. J. Jang, S.-D. Kim, W. Choi and Y. S. Chun, *Macromol. Symp.*, 2012, **312**, 34-42.
8. Y. Lin, V. Yakovleva, H. Chen, A. Hiltner and E. Baer, *J. Appl. Polym. Sci.*, 2009, **113**, 1945-1952.
9. Z. S. Petrovic, J. Budinski-Simendi, V. Divjakovi and Z. e. Scaronkrbi, *J. Appl. Polym. Sci.*, 1996, **59**, 301-310.

10. R. E. Robertson and D. R. Paul, *J. Appl. Polym. Sci.*, 1973, **17**, 2579-2595.
11. M. Mirabella Francis, in *Applications of Scanned Probe Microscopy to Polymers*, American Chemical Society, 2005, vol. 897, ch. 16, pp. 224-238.
12. B. Qiu, F. Chen, Y. Shangguan, L. Zhang, Y. Lin and Q. Zheng, *RSC Advances*, 2014, **4**, 58999-59008.
13. G.-J. Zhong and Z.-M. Li, *Polymer Engineering & Science*, 2005, **45**, 1655-1665.
14. R. R. Tiwari and D. R. Paul, *Polymer*, 2011, **52**, 4955-4969.
15. D. W. Van Krevelen and K. Te Nijenhuis, in *Properties of Polymers (Fourth Edition)*, Elsevier, Amsterdam, 2009, pp. 525-597.
16. R. H. Olley and D. C. Bassett, *Polymer*, 1982, **23**, 1707-1710.
17. P. Doshev, G. Lohse, S. Henning, M. Krumova, A. Heuvelsland, G. Michler and H.-J. Radusch, *J. Appl. Polym. Sci.*, 2006, **101**, 2825-2837.
18. R. H. Olley, A. M. Hodge and D. C. Bassett, *Journal of Polymer Science: Polymer Physics Edition*, 1979, **17**, 627-643.
19. D. R. Norton and A. Keller, *Polymer*, 1985, **26**, 704-716.
20. J. X. Li, W. L. Cheung and C. M. Chan, *Polymer*, 1999, **40**, 2089-2102.
21. J. Park, K. Eom, O. Kwon and S. Woo, *Microsc. Microanal.*, 2001, **7**, 276-286.
22. B. K. Kim and I. H. Do, *J. Appl. Polym. Sci.*, 1996, **60**, 2207-2218.
23. J. Karger-Kocsis, A. Kalló and V. N. Kuleznev, *Polymer*, 1984, **25**, 279-286.
24. M. Kontopoulou, W. Wang, T. G. Gopakumar and C. Cheung, *Polymer*, 2003, **44**, 7495-7504.
25. H. Tan, L. Li, Z. Chen, Y. Song and Q. Zheng, *Polymer*, 2005, **46**, 3522-3527.
26. G. Grestenberger, G. Potter and C. Grein, *Express Polymer Letters*, 2014, **8**, 282-292.
27. M. Ono, K. Nakajima and T. Nishi, *J. Appl. Polym. Sci.*, 2008, **107**, 2930-2943.
28. K. Min, J. L. White and J. F. Fellers, *Polymer Engineering & Science*, 1984, **24**, 1327-1336.
29. M. V. Tsebrenko, N. M. Rezanova and G. V. Vinogradov, *Polymer Engineering & Science*, 1980, **20**, 1023-1028.
30. B. K. Kim and I. H. Do, *J. Appl. Polym. Sci.*, 1996, **61**, 439-447.
31. J. Karger-Kocsis and V. N. Kuleznev, *Polymer*, 1982, **23**, 699-705.
32. L. D'Orazio, C. Mancarella, E. Martuscelli and G. Sticotti, *J. Mater. Sci.*, 1991, **26**, 4033-4047.
33. L. D'Orazio, C. Mancarella, E. Martuscelli and F. Polato, *Polymer*, 1991, **32**, 1186-1194.
34. A. L. N. D. Silva, M. C. G. Rocha, F. M. B. Coutinho, R. Bretas and C. Scuracchio, *J. Appl. Polym. Sci.*, 2000, **75**, 692-704.
35. S. H. Wu, *Polymer*, 1985, **26**, 1855.
36. C. B. Bucknall, *Journal of Elastomers and Plastics*, 1982, **14**, 204-221.
37. B. Z. Jang, D. R. Uhlmann and J. B. Vander Sande, *J. Appl. Polym. Sci.*, 1985, **30**, 2485-2504.
38. B. Z. Jang, D. R. Uhmann and J. B. Vander Sande, *Polym. Eng. Sci.*, 1985, **25**, 643.
39. A. v. d. Wal, A. J. J. Verheul and R. J. Gaymans, *Polymer*, 1999, **40**, 6057-6065.

The properties of the polyolefins blends depend not only the composition but also on the morphology.